IEEE Access
Multidisciplinary ⋮ Rapid Review ⋮ Open Access Journal

Received April 23, 2020, accepted May 30, 2020, date of publication June 2, 2020, date of current version June 18, 2020.

Digital Object Identifier 10.1109/ACCESS.2020.2999478

Gear Backlash Detection and Evaluation Based on Current Characteristic Extraction and Selection

QICHAO YANG, TAO LIU, XING WU, AND YUNNAN DENG

Key Laboratory of Vibration and Noise under Ministry of Education of Yunnan Province, Kunming University of Science and Technology, Kunming 650500, China

Corresponding author: Xing Wu (xwu@kust.edu.cn)

This work was supported in part by the National Key Research and Development Plan of China under Grant 2018YFB1306103, in part by the National Natural Science Foundation of China under Grant 51875272 and Grant 51675251, and in part by the Key Scientific Research Project of Yunnan Province under Grant 2017FA028.

ABSTRACT Motor Current Signal Analysis (MCSA) is widely used in the monitoring of electric motors, but few researchers applied it in the transmission system because of the fault information loss and aliasing of current signals. The purpose of the research is to analyze the influence of the gear backlash under different size effect on the current signal from the permanent magnet synchronous motor (PMSM). And it supplies a convenient route to detect the gear backlash more economy. In most cases, the current of PMSM is usually changed with the operating states, which may relate with rotor speed, load and gear backlash. So, it is important to extract the sensitive features under different states. Here, the stable speed and variable speed states are considered at first. At the steady stage, multiple features are extracted from current signals under variable backlash. And fisher discriminant analysis (FDA) is introduced to evaluate and select the most sensitivity features for backlash are selected. Then, features at variable speed states are extracted. Because the transient change of the current frequency and phase adjustable, it is very difficult to obtain the steady state response characteristic. In this paper, the inverse of the time difference between the positive peaks of the signal at this phase is utilized as the characteristic index describing phase. Furthermore, the polynomial principle is combined to enhance the characteristics of the extracted features. Therefore, the mapping relationship between the backlash and the current signal of the servo motor is established under different speed stages. The results show that by monitoring the motor current, it is feasible and effective to distinguish the different backlash of the meshing gear.

INDEX TERMS MCSA, gear backlash, servo motor, current signal, feature extraction.

I. INTRODUCTION

The dynamic performance of gears has an important impact on the entire machine [1]. Gears are one of the core components of mechanical equipment, and its state directly affects the performance of the entire mechanical equipment. Therefore, many scholars have carried out research and achieved some achievements. With the rapid development of mechanical automation, with the increase in power and speed, friction [2], [3], scratches [4], [5], pitting, broken teeth [6] and misalignment [7], [8] of gears have become major concerns of scholars [9]. Research of gear fault diagnosis is of extreme significance to industrial production and social life.

The associate editor coordinating the review of this manuscript and approving it for publication was Youqing Wang.

More and more studies show that the existence of the backlash will seriously affect the stability and accuracy of the gear system, and it is extremely important to research and diagnose the gear backlash. Reference [10] proposed a multi-degree-of-freedom dynamic model of the gear system. This model considers the time-varying behavior of the backlash, the conclusion is that the initial backlash has a significant effect on the dynamic characteristics of the gear system. Reference [11] is shown that with the change of the backlash of the gear, there are always tooth meshing and separation on the back of the gear, and the backlash will significantly affect the gear's vibration and shock characteristics. Reference [12] is based on the fractal theory, by changing the backlash of gears to change the dynamic behavior of gears. It effectively reflects the dynamic characteristics of gears affected by changes in recoil. Reference [13] extended the incremental

harmonic balance method (IHBM) to the nonlinear dynamic analysis of a spur gear pair with backlash, and studied the effect of multi-order harmonics on the periodic solution. The above research has promoted the research on backlash, but the research is only based on model simulation, and the experimental conditions are too ideal.

Reliable gear fault diagnosis can not only reduce economic losses, but also reduce the risk of employee injury and death [14]–[16]. Research on gear fault monitoring has always been a hot topic, and research methods and signal media are also diverse. Generally speaking, fault detection and diagnosis methods can generally be divided into two categories, namely model-based methods and data-driven methods [17], [18]. Based on these two different approaches, scholars in gear research are also constantly innovating to detect and monitor the health of gears from various angles [19], [20].

Based on the actual requirements, this paper analyzes the effect of the backlash of the gear on the system based on the current signal analysis of the servo motor. Gear failure based on MCSA has been favored more and more in recent years due to their advantages such as low cost, easy acquisition of signals, and convenient implementation of field applications. The essence of MCSA is to analyze the current change caused by the output torque feedback to the motor stator [21]. Compared with traditional dynamic gear failure analysis, MCSA can not only reflect the fault information of the motor itself, but also detect the health status of the external equipment of the motor [22]. At present, scholars have studied the effect of gear, motor coupling and bearing on the motor current signal when there is a fault. For example, Reference [23] collected the motor stator current signal, determined the instantaneous amplitude and frequency based on the Local Mean Decomposition (LMD) method, and extracted the instantaneous amplitude sample entropy and the instantaneous frequency peak-to-peak value as the instantaneous performance indicators, then evaluate the performance of the servo motor. Reference [24] is based on the current signal of the feed motor of the CNC milling machine to monitor the tool groove break during end milling. Reference [25] based on three-phase current analysis, extracted characteristic indicators for gear fault detection and diagnosis. Reference [26] built a planetary gear fault feature extraction model based on deep neural networks, and verified the effectiveness of planetary gear fault identification. Reference [27] used dual-spectrum analysis of motor current signals to detect wear faults on spur gear tooth surfaces. Reference [28] analyzed the sideband spectrum of the current signal to realize the detection of shaft misalignment and imbalance faults. Reference [29] detected the planetary gearbox failure based on the resonance residue of the motor current signal. Reference [30] based on the statistical index of current spectrum realized the bearing fault detection of air-conditioning fan. Reference [31] used the frequency component of the stator current to estimate the torque, and identified a misalignment faults between the motor and the load. Although there are many studies on the detection of bearing and gear faults based on electrical signals, there are not many studies on gear backlash.

This paper analyzes and studies the effect of gear backlash on the system. Mainly for the identification and evaluation of spurring gears backlash failure in meshing teeth. For designing and building an experimental bench, collecting the current signals of the servo drive motor, extracting the time and frequency domain features reflecting the changes in the current signal [25], and establishing the mapping relationship between the backlash and the current signal. In the steady speed phase, multiple features are extracted from different backlash current signals, and the sensitivity is evaluated based on the FDA [32], [33] method to find the most sensitive state quantity for backlash. FDA is used to reduce the dimension of high-dimensional feature sets and retain significant features, providing the best low-dimensional representation. In many cases, the FDA solves the data dimensionality reduction problem better than the Principal Component Analysis (PCA) method. Although they all show nonlinearity, the FDA-based algorithm concept has been applied [34]–[36]. In the shifting phase, the reciprocal of the time difference between the positive peaks of the signals in the shifting phase is extracted as a characteristic index describing this phase. Combined with the polynomial principle, the extracted features are enhanced. The effect of the backlash on the shifting state is more clearly expressed.

The remainder of the paper is structured as follows. Section 2 describes the extraction of backlash fault features with electrical parameters. Section 3 conducts experiments by designing and building a test bench. The collected motor current signals are analyzed in Section 4. Finally, Section 5 presents the conclusions and perspectives of this work.

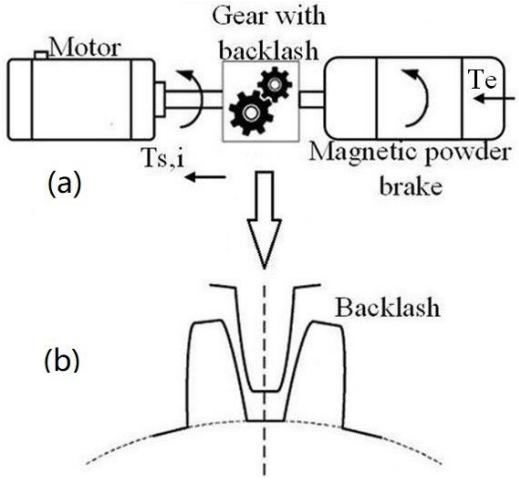

FIGURE 1. Variable tooth backlash test model.

II. FEATURE EXTRACTION OF BACKLASH FAULT BASED ON ELECTRICAL PARAMETERS

A. ELECTRICAL PARAMETER OF SERVO SYSTEM

Fig. 1 shows a schematic diagram of the test bench drive used. The driver consists of two spur gears mounted on a shaft,

each spur gear being supported by two ball bearings mounted on a bearing block. Specifically, it can divide into three parts. The power part is composed of a servo motor and its supporting driver and transformer. The main function of the motor shown in Fig. 1,(a) is to provide a power source for the system and drive the load to run. Connected to the motor output is a gear transmission system. The purpose of this experiment is to detect gear transmissions with backlash, as shown in part (b) of Fig. 1, gears with backlash. Fitted gears with backlash. The main components of this part A pair of meshing gears are connected by four bearing blocks and four couplings as a transmission part of the entire system. The output end of the gear transmission system is a load device. The load uses a magnetic powder brake. During the test, the magnetic powder brake can be adjusted in real time to change the load on the system. To collect current signals under different loads, more comprehensive information is used to evaluate the health status of the gear.

The PMSM is mainly composed of a fixed stator with three-phase windings and a rotor with permanent magnet poles. When three-phase alternating current is supplied to the stator windings, a rotating magnetic field is generated. The rotating magnetic field interacts with the permanent magnet poles on the rotor to generate electromagnetic torque and cause the synchronous rotation of the rotor. The three-phase windings of the stator is symmetrically distributed, the winding currents are recorded as i_a, i_b and i_c stator currents, and the phase difference is $2\pi/3$. To simplify the mathematical analysis of PMSM, a synchronous axis reference system defined by d and q axes is usually used. The d-axis is the axis of the permanent magnet poles, and the q-axis is perpendicular to the d-axis. In the d-q plane, the stator current is converted into an exciting current component to generate a magnetic flux and a torque current component to generate an electromagnetic torque. The conversion function is as follows:

$$\begin{bmatrix} i_d \\ i_q \end{bmatrix} = \sqrt{\frac{2}{3}} \begin{bmatrix} \cos\theta & \cos\left(\theta - \frac{2\pi}{3}\right) & \cos\left(\theta + \frac{2\pi}{3}\right) \\ -\sin\theta & -\sin\left(\theta - \frac{2\pi}{3}\right) & -\sin\left(\theta + \frac{2\pi}{3}\right) \end{bmatrix} \times \begin{bmatrix} i_a \\ i_b \\ i_c \end{bmatrix} \quad (1)$$

Here θ is the angular position of the rotor. Due to the orthogonality of i_{d} and i_q, the excitation magnetic field and electromagnetic torque can be adjusted separately.

$$\begin{cases} \psi_d = L_d i_d + \psi_f \\ \psi_q = L_q i_q \end{cases} \quad (2)$$

L_d and L_q are the inductances of the d and q axes, respectively, and are the flux linkages generated by the permanent magnet poles on the rotor. The electromagnetic torque is calculated using the following formula:

$$T_e = p\left(\psi_d i_q - \psi_q i_d\right) = p\left[\psi_f i_q + \left(L_d - L_q\right) i_d i_q\right] \quad (3)$$

p is the number of pole pairs. If PMSM is used to drive mechanical load T_l with reaction torque, the PMSM motion equation is:

$$T_e - T_l = J\frac{d\omega}{dt} + B\omega \quad (4)$$

J is the moment of inertia of the entire rotor, ω is the rotational speed, and B is the viscous friction coefficient.

Setting $i_d = 0$ is the most widely used closed-loop control strategy for PMSM [37]. By setting $i_d = 0$, the demagnetization of the permanent magnet caused by the armature reaction is avoided. According to equation(3), the electromagnetic torque is proportional to i_{q}. Therefore, it is easy to control the electromagnetic torque by changing the stator current. For example, if the known electromagnetic torque is T_e^*, the current i_{q}^* can be determined using equation(3), and the three-phase reference stator currents i_a^*, i_b^* and i_c^* are calculated as follows:

$$\begin{bmatrix} i_a^* \\ i_b^* \\ i_c^* \end{bmatrix} = \sqrt{\frac{2}{3}} \begin{bmatrix} \cos\theta & -\sin\theta \\ \cos\left(\theta - \frac{2\pi}{3}\right) & -\sin\left(\theta - \frac{2\pi}{3}\right) \\ \cos\left(\theta + \frac{2\pi}{3}\right) & -\sin\left(\theta + \frac{2\pi}{3}\right) \end{bmatrix} \begin{bmatrix} 0 \\ i_q^* \end{bmatrix} \quad (5)$$

B. SIGNAL ANALYSIS AT STEADY SPEED

1) FEATURE EXTRACTION AND ANALYSIS OF SIGNALS

When the gear fails, the amplitude and probability distribution of the time domain signal of the servo motor current will change, and the energy of different frequency components will change; therefore, the analysis of the current signal can detect the health status of the gear.

In order to obtain the effect of gear backlash on the motor current signal in a comprehensive manner, feature extraction is performed on the data set samples from the time domain and frequency domain, respectively. This paper uses the time domain and frequency domain features comprehensively, and extracts 14 time domain features (s1 to s14) and 15 frequency domain features (p1 to p15) from the collected servo motor current signals. As shown in Table 1, $x(i)$ is a time-domain sequence signal, $i = 1, 2, \ldots, N$, N are the number of sample points, X_k is the spectrum of signal $x(i)$, and $k = 1, 2, \ldots, N/2.56$ is the number of spectral lines. The parameters involved in the table, $PS[0] = |X_0|^2/N^2$, $PS[k] = 2|X_k|^2/N^2$, $f = 2.56fs * k/N$, $M = 1 + N/2$, $s0 = \min\{|x_1|, |x_2|, \cdots, |x_N|\}$

Table 1, the time domain characteristics s1 to s4, s11, s13, and s14 reflect the amplitude and energy of the time domain vibration, s5, s8 to s10, and s12 reflect the time series distribution of the time domain signal, and s6 is the standard of the time domain signal poor, s7 reflects the crest factor of the signal. The frequency domain characteristics p1 to p3 reflect the magnitude of the frequency-domain fluctuation energy, p4 to p6, p8, and p9 reflect the changes in the position of the main frequency band, p10 to p13 represent the degree of dispersion or concentration of the spectrum; p7 represents

TABLE 1. Time and frequency domain feature.

$s1=\max\{\lvert x_1\rvert,\cdots,\lvert x_N\rvert\}$	$s9=\frac{1}{N}\sum_{i=1}^{N}\left(\frac{x_i-s3}{s6}\right)^4$	$p3=\frac{\sum_{k=1}^{\frac{N}{2.56}}PS[k]f}{p1}$	$p11=\frac{\sum_{k=0}^{\frac{N}{2.56}}\left((f-p3)^3PS[k]\right)}{p6^3*N}$
$s2=\frac{1}{N}\sum_{i=1}^{N}\lvert x_i\rvert$	$s10=\frac{1}{N}\sum_{i=1}^{N}\left(\frac{x_i-s3}{s6}\right)^3$	$p4=\frac{\frac{1}{M}\sum_{k=0}^{\frac{N}{2.56}}(PS[k]-p2)^3}{\sqrt{\left(\frac{1}{M}\sum_{k=0}^{\frac{N}{2.56}}(PS[k]-p2)^2\right)^3}}$	$p12=\frac{\sum_{k=0}^{\frac{N}{2.56}}\left((f-p3)^4PS[k]\right)}{p6^4*N}$
$s3=\frac{1}{N}\sum_{i=1}^{N}x_i$	$s11=0.5(s1-s0)$	$p5=\frac{\frac{1}{M}\sum_{k=0}^{\frac{N}{2.56}}(PS[k]-p2)^4}{\left(\frac{1}{M}\sum_{k=0}^{\frac{N}{2.56}}(PS[k]-p2)^2\right)^2}$	$p13=\frac{\sum_{k=0}^{\frac{N}{2.56}}\sqrt{\left(\lvert f-p3\rvert\right)PS[k]}}{N\sqrt{p6}}$
$s4=\sqrt{\frac{1}{N}\sum_{i=1}^{N}x_i^2}$	$s12=\frac{s1}{s2}$	$p6=\sqrt{\frac{2.56\sum_{k=0}^{\frac{N}{2.56}}\left((f-p3)^2PS[k]\right)}{N}}$	$p14=\frac{1}{M}\sum_{k=0}^{\frac{N}{2.56}}(PS[k]-p1)^2$
$s5=\frac{s4}{s2}$	$s13=s1-s0$	$p7=\sqrt{\frac{\sum_{k=0}^{\frac{N}{2.56}}\left((f)^2*PS[k]\right)}{p1}}$	
$s6=\sqrt{\frac{1}{N}\sum_{i=1}^{N}(x_i-s3)^2}$	$s14=\left(\frac{1}{N}\sum_{i=1}^{N}\sqrt{\lvert x_i\rvert}\right)^2$	$p8=\sqrt{\frac{\sum_{k=0}^{\frac{N}{2.56}}\left(f^4*PS[k]\right)}{\sum_{k=0}^{\frac{N}{2.56}}\left(f^2*PS[k]\right)}}$	$p15=-\frac{\sum_{k=1}^{\frac{N}{2}}\left(\frac{\lvert X_k\rvert}{\sum_{k=1}^{\frac{N}{2}}\lvert X_k\rvert}*\log 2(\frac{\lvert X_k\rvert}{\sum_{k=1}^{\frac{N}{2}}\lvert X_k\rvert})\right)}{\log 2(\frac{N}{2}-1)}$
$s7=\frac{\max\{x_i\}}{\sqrt{\frac{1}{N}\sum_{i=1}^{N}x_i^2}}$	$p1=PS[0]+\sum_{k=1}^{\frac{N}{2.56}}PS[k]$	$p9=\frac{\sum_{k=0}^{\frac{N}{2.56}}\left(f^2*PS[k]\right)}{\sqrt{p1*\sum_{k=0}^{\frac{N}{2.56}}\left(f^4*PS[k]\right)}}$	
$s8=\frac{s1}{s4}$	$p2=\frac{p1}{M}$	$p10=\frac{p6}{p3}$	

the rms frequency of the signal, p14 represents the signal frequency variance, and p15 is the amplitude spectral entropy of the signal.

In addition, we also use empirical mode decomposition (EMD) to process the signal. After the signal is decomposed by EMD, a series of stable time-domain signals can be obtained. The decomposed IMF mode components represent the characteristic signals of different time scales contained in the original signal. Each IMF component can be regarded as a single frequency signal or an approximate narrow-band signal, reflecting the modes from high frequency to low frequency respectively. Here, we use EMD to process the current signal and retain the first to third layers of IMF, and then square the sum of the retained IMF and then average, so that we can obtain 3 characteristic values used to describe the signal, emd1 to emd3.

Finally, we also analyzed the signal from the perspective of energy classification to obtain the eigenvalues. Wavelet packet decomposition can decompose different frequency bands of signals, and wavelet packet decomposition can adaptively select corresponding frequency bands according to signal characteristics, which are a finer decomposition method. Here, the signal is decomposed in 3 layers of wavelet packets, so that 8 different energy bands can be obtained. Taking the energy ratio of each energy band as an indicator for the signal description, to obtain 8 eigenvalues from wpd1 to wpd8. A total of 40 various types of features are used to describe the state of the system.

Because these characteristics are different in sensitivity to backlash failure. Therefore, it is necessary to select sensitive features that are closely related to the fault and eliminate redundant or irrelevant features to improve the performance of discrimination.

2) FEATURE EVALUATION AND SELECTION BASED ON FDA

The principle of the Fisher criterion for determining feature correlations is derived from the FDA method. The FDA method is a classified linear model. The basic idea of this method is to project the sample points onto a straight line or a hyperplane, so that the variance of the samples of the same type of samples is minimized after projection, and the difference of the sample mean between samples of different categories is as large as possible.

For a multi-classification problem, the FAD method will obtain the between-class divergence matrix S_B and the within-class divergence matrix S_W projected onto the vector w, and then solve the following objective function to obtain w, that is,

$$\max_w f(w) = \frac{w^{\mathrm{T}} S_B w}{w^{\mathrm{T}} S_W w} \tag{6}$$

This means that after all samples are projected to w, the variance of similar samples is made as small as possible, and the difference between the mean values of the samples of different types is as large as possible. The inter-class divergence matrix S_B and the intra-class divergence matrix S_W are calculated based on the sample data. Suppose the training sample set $X = [x_1, x_2, \cdots, x_n]$ has K classes, and the $i-th$ sample x_i is projected onto the straight line w to obtain y_i, that is $y_i = w^T x_i, i = 1, \cdots, n$. The inter-class distance after projection to w can be obtained by subtracting the entire sample average after projection from the samples after each class projection, and then adding these differences, that is,

$$\sum_{k=1}^{K} n_k \left(\mu_k^w - \mu^w\right)\left(\mu_k^w - \mu^w\right)^{\mathcal{T}} = w^T \left(\sum_{k=1}^{K} n_k \left(\mu_k - \mu\right)\left(\mu_k - \mu\right)^{\mathcal{T}}\right) w \tag{7}$$

In the formula, μ_k and μ_k^w represent the mean values of the samples of the $k-th$ sample before and after the projection, that is, $\mu_k^w = \frac{1}{n_k}\sum_{i\in C_k} y_i = w^T \frac{1}{n_k}\sum_{i\in C_k} x_i = w^T \mu_k$; μ and μ^w represent the average values of all samples before and after projection, that is, $\mu^w = \frac{1}{n}\sum_{k=1}^{K} n_k \mu_k^w = w^T\left(\frac{1}{n}\sum_{k=1}^{K} n_k \mu_k\right) = w^T \mu$, C_k represents the subscript set of the $k-th$ sample, and n_k represents the number of the $k-th$ sample.

The intra-class distance after projection to w can be obtained by subtracting the average value of the projected samples from each projected sample and then adding these differences, that is,

$$\sum_{k=1}^{K}\sum_{i=C_k}\left(y_i - \mu_i^{\mathrm{w}}\right)\left(y_i - \mu_i^{w}\right)^{\mathcal{T}} = w^{\mathcal{T}}\left(\sum_{k=1}^{K}\sum_{i\in C_k}\left(x_i - \mu_k\right)\left(x_i - \mu_k\right)^{\mathcal{T}}\right) w \tag{8}$$

For equations (7) and (8) above, if

$$S_{\mathrm{W}} = \sum_{k=1}^{K}\sum_{i\in C_k}\left(x_i - \mu_k\right)\left(x_i - \mu_k\right)^{T} \tag{9}$$

$$S_B = \sum_{k=1}^{K} n_k \left(\mu_k - \mu\right)\left(\mu_k - \mu\right)^{\mathrm{T}} \tag{10}$$

This gives the objective function of the FDA method.

If the objective function is required to be solved, it can be converted into the following problem and then solved, that is,

$$S_B w = \lambda S_W w \tag{11}$$

Equation (11) is a generalized eigenvalue problem, where λ is a generalized eigenvalue and w is a generalized eigenvector. If S_w is invertible, there is $S_W^{-1} S_B w = \lambda w$, and the problem becomes to find the eigenvalues of matrix $S_W^{-1} S_B$.

Since the FDA method is a classification algorithm, it cannot be used to evaluate the relevance of features. The Fisher criterion is a method for evaluating the correlation of features. It borrows the idea of the FDA method, that is, the Fisher criterion also uses the idea that the variance of the same sample is as small as possible, and the difference between the sample mean between the similar samples is as large as possible to calculate the feature correlation.

Fisher criterion For the $i-th$ feature f_i, its values belong to K classes. For the value of f_i, the S_B and S_W are calculated separately as in the FDA method. The calculation process is as follows. First calculate S_W, that is

$$S_W = \sum_{k=1}^{K} S_k \tag{12}$$

In the formula, $S_k = \sum_{j\in C_k}\left(f_{ij} - \mu_k\right)^2$, $\mu_k = \frac{1}{n_k}\sum_{j\in C_k} f_{ij}$, C_k represents the index set of the $k-th$ sample, and n_k represents the number of the $k-th$ sample. Second, calculate S_B, that is

$$S_B = \sum_{k=1}^{K} n_k(\mu_k - \mu) \tag{13}$$

where $\mu_k = \frac{1}{n_k}\sum_{j\in C_k} f_{ij}$, $\mu = \frac{1}{K} n_k \mu_k$, for multiple features, S_B and S_W are calculated as matrices. Finally calculate the

correlation Sensitivity$_i$ of the features, that is,

$$\text{Sensitivity}_i = \frac{S_B}{sum\,(S_W)} \tag{14}$$

If Sensitivity is large, it means that the variance of similar samples may be small, while the mean of samples between non-similar samples may be large, which means that the discriminability of the samples is better.

C. SIGNAL ANALYSIS DURING SHIFTING PHASE

The speed change phase of the signal is a very important part of the system operation. This phase contains a lot of information. Various information can be seen in the time-domain signal, and changes in speed and load can be reflected in the signal. According to the working conditions, the A-phase signals of the three-phase current signals of the motor with variable backlash of 0.25mm, 0.50mm, and 0.75mm in the variable-speed stage were extracted. The signal intercepted during the descent phase is the process of the motor's operating state from steady speed to zero speed, and the signal intercepted during the ascent phase is the process of the motor's operating state from speed to zero speed. The first wave peak when the motor is started is selected as the reference point, and the signals of three different backlash operating conditions are referenced as the reference point for time-domain overlap, and the amplitude and frequency change is analyzed from the angle of speed. In order to reflect this difference more clearly and intuitively, each one takes the peak point of the time-domain waveform of the current signal during the variable-speed phase as a reference, and takes one-time interval between the positive peak points of the variable-speed signal as a description of how fast this waveform changes. Finally, polynomial fitting is used to enhance the effectiveness of the extracted indicators.

For polynomial fitting, given a set of data $\{(x_i, y_i)\,, i = 0, 1, 2, \cdots, N\}$, a polynomial model is used to describe the data set, and the fitting goal is for a polynomial model of order n of the form $y(x) = f(a, x) = a_1x^n + a_2x^{n-1} + \cdots + a_nx + a_{n+1}$, find the parameter $a_1, a_2, \cdots, a_n, a_{n+1}$ to minimize the following χ^2 amount.

$$\begin{aligned}\chi^2 &= \sum_{i=1}^{N}\left(\frac{y_i - f\,(a, x_i)}{\Delta y_i}\right)^2 \\ &= \sum_{i=1}^{N}\left(\frac{y_i - \left(a_1x_i^n + a_2x_i^{n-1} + \cdots + a_nx_i + a_{n+1}\right)}{\Delta y_i}\right)^2\end{aligned} \tag{15}$$

Under the assumption that $\Delta y_i = \Delta_y$ is constant, the solution that minimizes (15) is

$$\hat{a} = \mathbf{V}/\mathbf{y} \tag{16}$$

Among them, $\mathbf{V} = \begin{bmatrix} x_1^n & x_1^{x-1} & \cdots & x_1 & 1 \\ x_2^n & x_2^{n-1} & \cdots & x_2 & 1 \\ \vdots & \vdots & \ddots & \vdots & \vdots \\ x_N^n & x_N^{n-1} & \cdots & x_N & 1 \end{bmatrix}$, $\widehat{\mathbf{a}} = \begin{bmatrix} \hat{a}_1 \\ \hat{a}_2 \\ \vdots \\ \hat{a}_{n+1} \end{bmatrix}$, $\mathbf{y} = \begin{bmatrix} y_0 \\ y_0 \\ \vdots \\ y_N \end{bmatrix}$, $\mathbf{V}$ is the Vandermonde matrix, and the uncertainty (dispersion) of $\widehat{\mathbf{a}}$ is $\sigma(\hat{a}) = diag\left(\left(\mathbf{V}^{\mathrm{T}}\mathbf{V}\right)^{-1}\right)^{\frac{1}{2}} \cdot \begin{bmatrix} \Delta_y \\ \Delta_y \\ \vdots \\ \Delta_y \end{bmatrix}$.

The characteristics extracted from the time-domain signal during the gear shift phase are curve-fitted using the above polynomial theory. Finally, three curves under different backlash are obtained, and the coefficients of the curves are used as the criterion for different gear backlash discrimination during the gear shift phase.

D. DATA PROCESSING FLOW BASED ON CURRENT SIGNAL

The motor operation process includes a variety of operation modes, which can be simply described as three types, the acceleration operation process, the stable operation process, and the deceleration operation process. For different running states, this article adopts different analysis methods. The analysis process is showed in Fig.2. For the collected current signals under different operating conditions, the current signal is first divided into a steady-time signal and a variable-speed signal, and the signal is divided according to the amplitude change of the current time-domain signal. The features extracted at steady and variable speed were evaluated using the FDA. Specific theoretical analysis methods are detailed in Sections B and C.

III. MOTOR CURRENT TEST OF GEAR TRANSMISSION SYSTEM

Based on the principle of gear meshing, analyze the cause of the backlash of the meshing teeth, and build a test bench, as showed in Fig. 3. It consists of a servo motor and its supporting driver, transformer, etc. The main function of the motor is to provide a power source for the system and drive the load to rotate. Connected to the motor output is a gear transmission system. The main part of the transmission part is a pair of meshing gears connected by four bearing blocks and four couplings. The load device is a magnetic powder brake. The magnetic powder brake can be adjusted to change the load in order to collect signals under different loads and obtain more comprehensive working condition data. The data acquisition system includes sensors, acquisition cards, signal conversion devices and computer systems. The signal collected this time is a three-phase current signal output from the driver to the servo motor. The main technical parameters of the test bench are shown in Table 2.

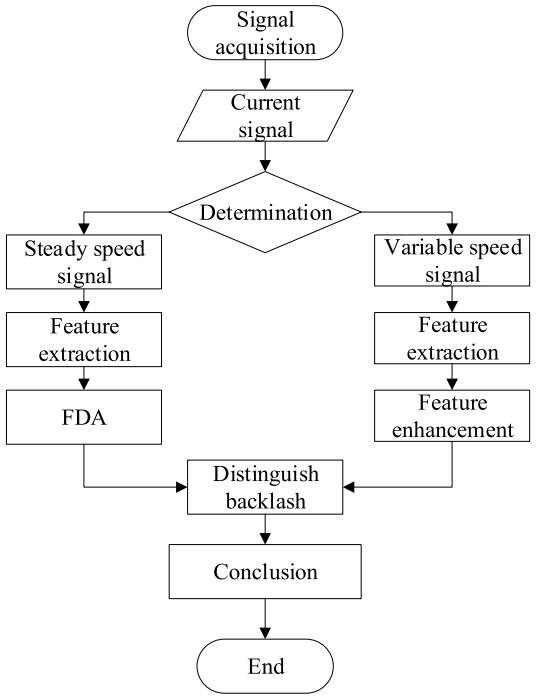

FIGURE 2. The left side is the data processing for the steady speed state by the FDA method, and the right side is the polynomial fitting method to enhance the characteristics of the speed change state. In order to realize the identification of tooth backlash in two states of steady speed and variable speed.

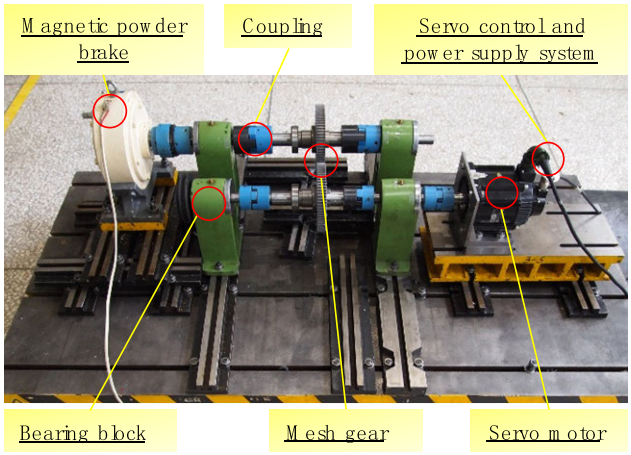

FIGURE 3. Backlash and servo system test bench.

TABLE 2. Test bench technical parameters.

AC Drive	Power 1.8Kw	Speed 1000rpm
Gear drive	Transfer method	Gear drive
	Meshing coefficient	/
	Thread angle /(°)	0
	Speed frequency /Hz	16.67
	Meshing frequency /Hz	1250
load(DC)	load	0~18.75N.m

For each test, the backlash is set quantitatively before data collection. After analyzing the actual working conditions

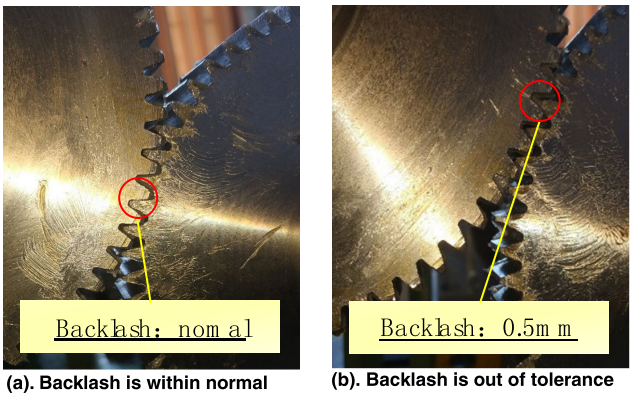

(a). Backlash is within normal range

(b). Backlash is out of tolerance

FIGURE 4. Backlash gear.

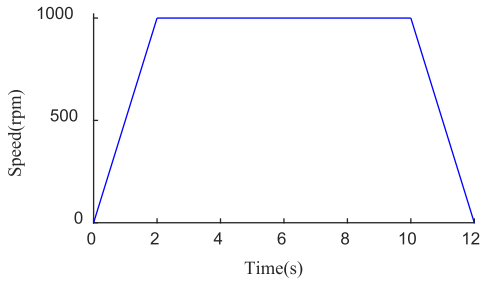

FIGURE 5. Test speed curve.

in this test, the feeler gauge method was selected as the side measurement method for measuring the gear backlash. Fig. 4 shows the meshing gear, (a) is within the standard backlash range, and (b) is the backlash is greater than the standard range, and the measured size is 0.5mm. The test simulates the backlash conditions caused by gear wear or mounting errors.

There are two operating variables in the test: ① Change the tooth backlash; ② Change load.

Table 3 shows the test conditions. For different backlash and different loads, the motor speed is constant at 1000 rpm, and the backlash starts at 0.25mm. There are 3 kinds of backlash working conditions: 0.25mm, 0.50mm, 0.75mm. For each backlash operating condition, there are four load conditions: 0N.m (no load), 6.25N.m, 12.5N.m, and 18.75N.m.

TABLE 3. Test condition information table.

Backlash(mm)	Speed (rpm)	load 1 (N.m)	load 2 (N.m)	load 3 (N.m)	load 4 (N.m)
0.25	1000	18.75	12.50	6.25	0
0.50	1000	18.75	12.50	6.25	0
0.75	1000	18.75	12.50	6.25	0

A total of 12 sets of data were collected throughout the test process, three backlash conditions, and four loads for each backlash. Each set of data contains the current signal of the gear system's stable forward and reverse and variable speed

operation. In the next section, In Section IV, the collected current signals will be analyzed, feature quantity will be extracted, and the effect of backlash on the system will be described.

The test acquisition software is NI SignalExpress2015 from NI Corporation of the United States. LabVIEW_SE is mainly used for waveform acquisition, generation, analysis, comparison, recording, import and export of data. The motor is a Yaskawa permanent magnet synchronous motor, and the current sensor is a ZHTK25 open-close current transformer produced by Nanjing Zhenhengtong Electronics Co., Ltd. The data acquisition card is NI 9215, and the acquisition box is an NI CompactDAQ_8-slot Ethernet chassis.

IV. TEST SIGNAL ANALYSIS

A. TEST SIGNAL

In order to verify the relationship between load and a backlash, a test with a backlash of 0.25mm, the speed of a1000rpm, load of 18.75Nm, 12.5Nm, 6.25Nm, and no-load (0N.m) conditions were performed first; then, the load and speed were fixed, change the backlash between the gears, and collect the current signal. When the motor is running, because the three-phase electric power is symmetrically distributed, a single-phase current signal can be selected for analysis. Each test motor has undergone the process of "starting-acceleration-steady speed-down stop-reverse acceleration-steady speed-down stop". Here, the phase A current of each backlash is selected as the counter signals analyzed by the system.

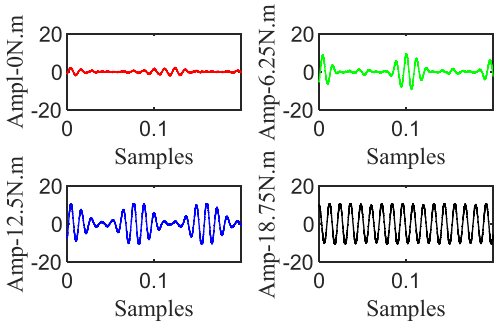

FIGURE 6. Backlash of 0.25mm-4 loads.

B. EFFECT OF LOAD AND BACKLASH ON THE SYSTEM

1) CASE1: SAME BACKLASH——DIFFERENT LOADS

In the test, there are 4 kinds of load conditions. Under the same backlash, the current time domain signals of different loads are given in Fig. 6, Fig. 8, Fig. 10. From the given current time domain signal, the load has a great influence on the current waveform amplitude. From the given current time domain signal, the load has a significant influence on the current waveform amplitude. As the load increases, the time domain signal amplitude changes from small to large, and the current waveform changes from intermittent to periodic harmonics. Fig. 7, Fig. 9, Fig. 11 shown the corresponding frequency distribution.

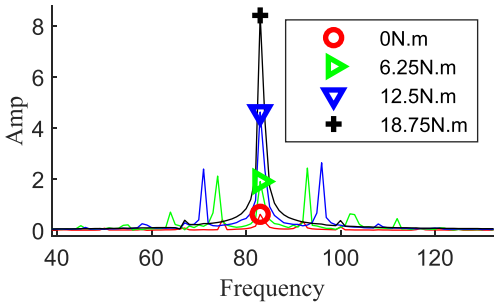

FIGURE 7. Backlash of 0.25mm-4 loads.

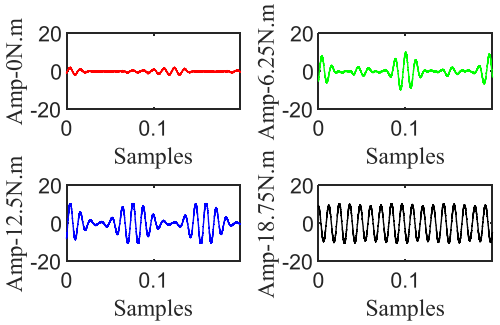

FIGURE 8. Backlash of 0.50mm-4 loads.

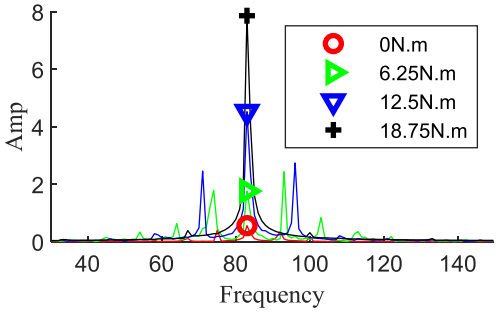

FIGURE 9. Backlash of 0.50mm-4 loads.

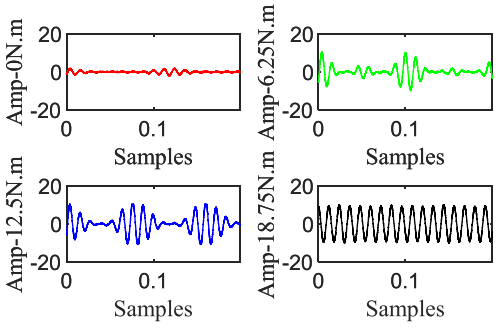

FIGURE 10. Backlash of 0.75mm-4 loads.

The signal given above is the effect of the gear on the current signal of the servo system with the gear as the single variable under the same backlash of the gear. It can be seen in the figure that the change of the load is mainly reflected on the amplitude of the current signal. With the continuous

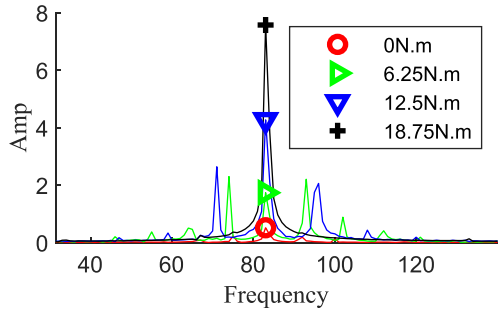

FIGURE 11. Backlash of 0.75mm-4 loads.

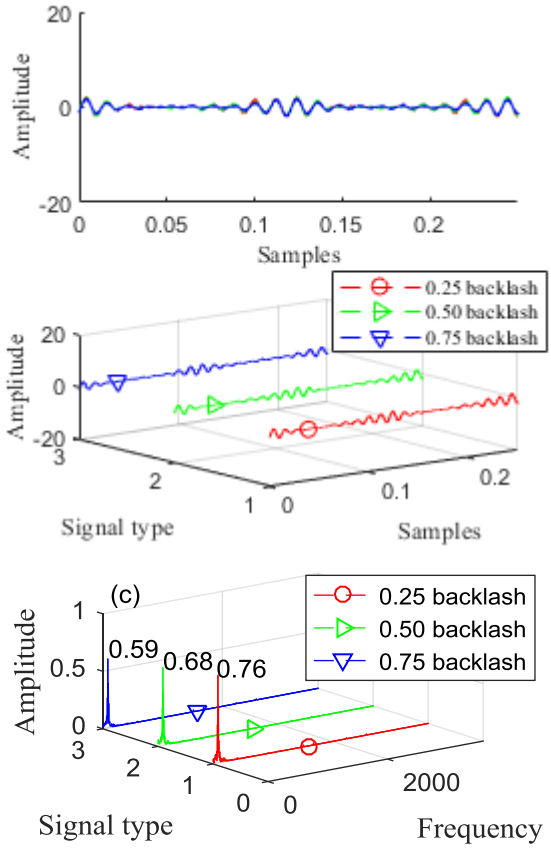

FIGURE 12. 0N.m load-different backlash.

increase of the load, the time domain waveform of the current signal changes from small amplitude and irregular waveform to large waveform amplitude, and tend to stabilize the standard sine wave. In the frequency domain, when the load is relatively small, many small harmonics are flooded around the main frequency, and the main peak amplitude is very small. When the load gradually increases, the harmonics near the main peak gradually decrease and the amplitude gradually increases. When the load is increased to 18.75N.m, there are basically no harmonics near the main peak. Comparing Fig. 7, Fig. 9 and Fig. 11, the backlash of the tooth increases, and the amplitude of the main peak of the current signal decreases.

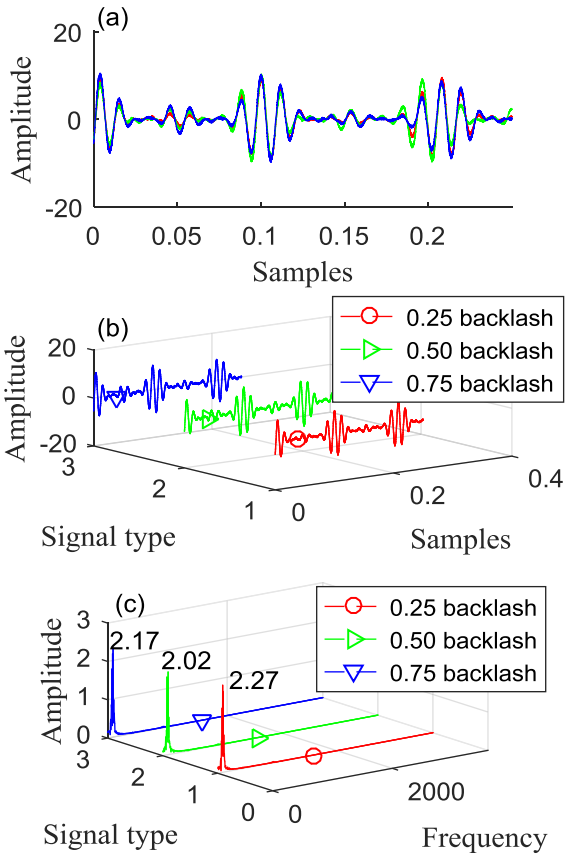

FIGURE 13. 6.25N.m load-different backlash.

2) CASE2:SAME LOAD——DIFFERENT BACKLASHES

In the illustrated current signal, under the condition that the test bench runs at a stable speed, the load is constant, and the gear tooth backlash is changed. Signal discrimination is very inconspicuous, and only a small gap can be seen in the amplitude of the time domain signal. Fig. 12-15, (a) is the time domain overlap of the three backlash current signals, (b) is the spatial display of (a), and (c) is the spectrum of the three signals. Under a small load, the waveform of the current signal appears as an exponentially decaying continuation signal of a sine wave. Fig. 12 and Fig. 13 show the time domain signal of the current signal under a small load. The difference between the waveform and amplitude of the current signal and the signal under a large load is very obvious. Especially when the system is running at no load, the current amplitude becomes very small. As the load increases, the current waveforms showed in Fig. 14 and Fig. 15 shown that each peak has a large amplitude.

To the right of the time domain signal is the spectrum of the current signal, with the load as a single variable. Looking at several figures, as the load becomes smaller, the current signal in the frequency spectrum appears more and more obvious around the main frequency, and the amplitude is decreasing. From the analysis of each spectrogram alone, the backlash is regarded as a single variable, and it can be seen that there is

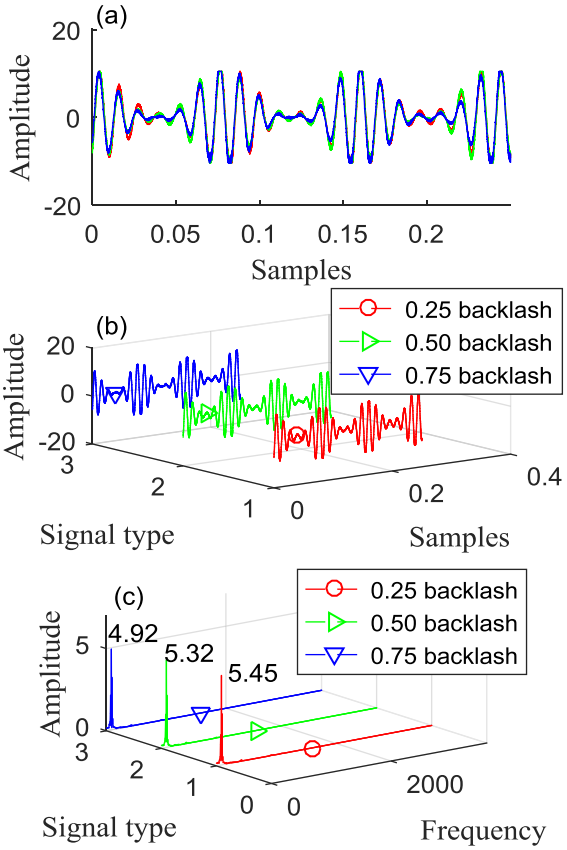

FIGURE 14. 12.5N.m load-different backlash.

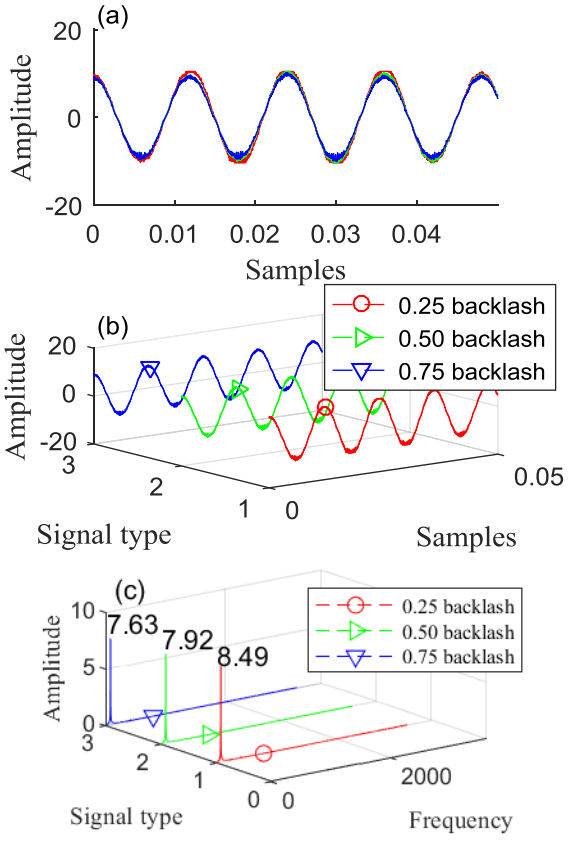

FIGURE 15. 18.75N.m load-different backlash.

a large amplitude at the frequency of 83Hz, and the different backlash shows the amplitude difference in signal strength. There are some tiny protrusions beside the main peak. It can be seen that the backlash does have an effect on the current signal.

Aiming at the motor current signals collected under various working conditions, this paper selects the current signals under steady-state operation and with a load of 18.75N.m for extracting features. The obtained signal is divided into segments of length N, as showed in Fig. 16. In this paper, the time-domain signal with a total length of 2.5s is divided into 25 segments with a length of 0.1s. The data set of different backlash under the same load is composed of 3×25 samples. That is, 25 samples are taken from three different backlash. The waveform of the current signal during the steady-speed operation of each backlash is shown in the right figure of Fig. 16. The signals are processed by using the method of processing signals in Table 1. Then use the Fisher discrimination criterion introduced in II.B.2 to screen and discriminate signal features.

As shown in Fig. 17, the sensitivity ranking of different feature classes, Table 4 is a ranking table of the sensitivity of all 40 features to the backlash. Among the extracted features, the first four features have higher sensitivity to the backlash of gears, and the fifth to tenth features gradually decrease in sensitivity. The characteristic sensitivity curve is shown in the figure. The sensitivity of the time domain signal s4 rms and s6 standard deviation to the gear backlash is better, and the frequency domain characteristic p1 spectrum total value and p2 mean frequency have better sensitivity to the gear backlash. These features had better recognition ability of backlash. However, the average sensitivity of s3, wpd2, and p3 in several experiments was lower, and the performance was the worst. 1 to 4th characteristics effectively describe the state of the system and can be used as a characteristic quantity to describe the effect of backlash on gears.

For the analysis of three types of backlash under 12.5Nm load, three types of backlash under 6.25Nm and three types of backlash under no-load conditions, the analysis methods are the same as those under the above conditions, so they are not one by one Narrative, the analysis results of different backlash conditions for these three load conditions are given below.

3) CASE3: VARIABLE SPEED STAGE

In this paper, the current signal collected by the servo motor with a load of 18.75N.m and speed of 1000rmp is selected to analyze the variable speed stage. As shown in Fig.20 and Fig. 22, when the backlash is equal to 0.25mm, 0.50mm, and 0.75mm, the A-phase signal of the three-phase current of the motor in the variable speed phase is extracted. In the phase of signal deceleration and descent, the signals under three different backlash operating conditions are processed according

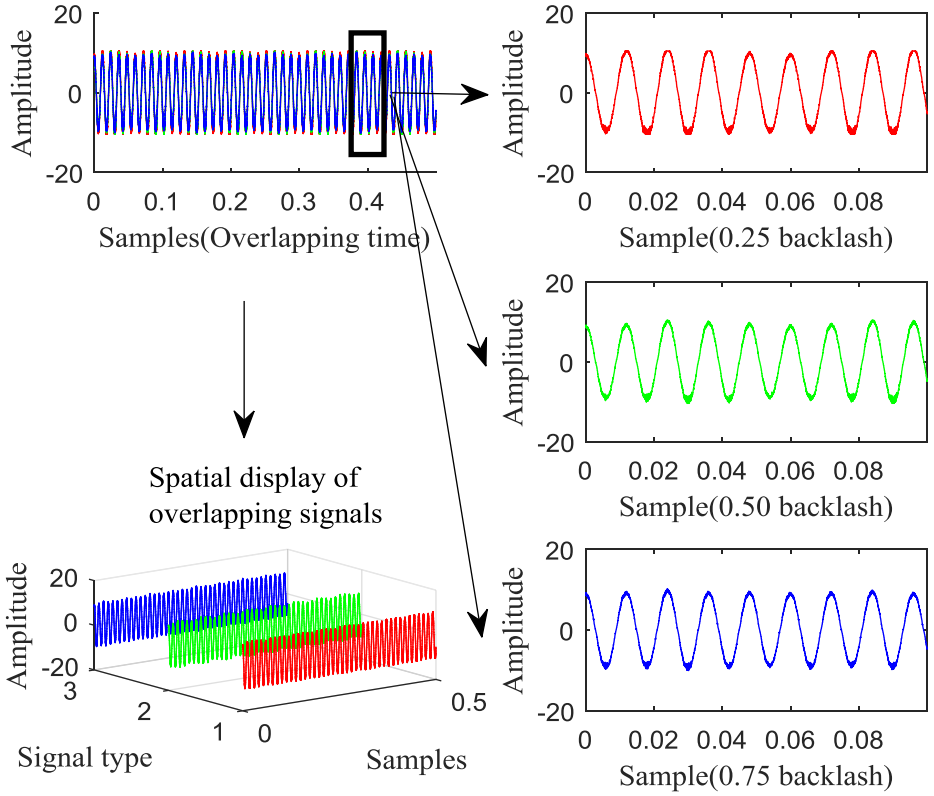

FIGURE 16. Segmentation of current signals.

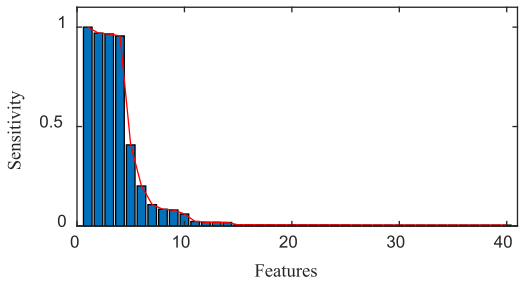

FIGURE 17. Ranking of different feature sensitivities.

to the method in II.C, and the time domain overlap of deceleration and descent in Fig. 23 is obtained. In the time domain signal diagram, observe the changes from the current signals overlapping in time. The frequency of the current changes is different. The signal of the red line obviously reaches the next peak point in a shorter time than the other two-phase signals. That is, when the gear backlash is 0.25mm, the frequency changes the fastest, the gear backlash is 0.50mm second, and the gear backlash is 0.75mm, the slowest change. This paper takes the reciprocal of the time interval between the peaks of the signal during the shift phase as an index to describe the speed of this waveform transformation. In Fig. 25, it can be observed that under different tooth backlash, the three curves are different, and the speed of frequency changes is different.

TABLE 4. 18.75N.m feature sensitivity ranking.

Ranking	Feature	Sensitivity	Ranking	Feature	Sensitivity
1	s6	1.00000	21	p11	0.00516
2	p1	0.96995	22	emd1	0.00509
3	p2	0.96566	23	emd2	0.00507
4	s4	0.95572	24	wpd8	0.00506
5	s2	0.40763	25	emd3	0.00495
6	s14	0.20102	26	s5	0.00454
7	p14	0.10733	27	wpd5	0.00446
8	s12	0.08404	28	p7	0.00442
9	s7	0.08031	29	wpd3	0.00441
10	s8	0.06014	30	wpd7	0.00438
11	p10	0.02257	31	wpd6	0.00437
12	s11	0.01855	32	wpd1	0.00437
13	s13	0.01855	33	s10	0.00437
14	s1	0.01748	34	p5	0.00436
15	wpd4	0.00592	35	p4	0.00435
16	p13	0.00563	36	p9	0.00435
17	p8	0.00548	37	p15	0.00435
18	p6	0.00546	38	s3	0.00435
19	p12	0.00520	39	wpd2	0.00434
20	s9	0.00518	40	p3	0.00434

In the acceleration rising phase of the signal, the processing method is the same as that of the deceleration falling signal. The results are shown in Fig. 24 and Fig. 26. The reciprocal of the time interval between the time domain signal and the peak point is used as an index, and the result opposite to the change rule of the signal during the deceleration and descent phase is obtained.

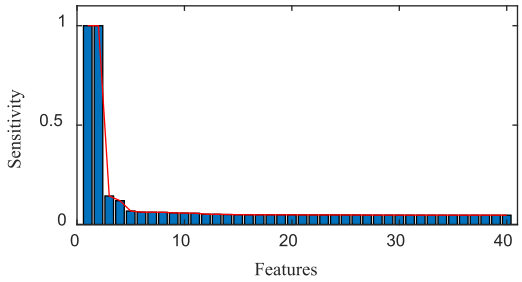

FIGURE 18. Feature sensitivity ranking.

TABLE 5. 12.5N.m feature sensitivity ranking.

Ranking	Feature	Sensitivity	Ranking	Feature	Sensitivity
1	s11	1	21	emd3	0.048403
2	s13	1	22	emd1	0.048371
3	wpd7	0.143635	23	emd2	0.048363
4	wpd8	0.119997	24	p7	0.048340
5	s1	0.067974	25	p10	0.048283
6	p4	0.062555	26	wpd6	0.048167
7	p5	0.062089	27	p8	0.047576
8	s5	0.061587	28	p13	0.047507
9	s8	0.058584	29	p6	0.047475
10	s14	0.057564	30	p9	0.047435
11	p14	0.056947	31	p12	0.047295
12	s12	0.052163	32	wpd4	0.047292
13	s2	0.051779	33	wpd5	0.047285
14	s9	0.050506	34	p11	0.047247
15	s10	0.049532	35	p3	0.047190
16	s7	0.048966	36	p15	0.047179
17	s6	0.048911	37	wpd1	0.047166
18	s4	0.048898	38	wpd2	0.047070
19	p2	0.048881	39	wpd3	0.047066
20	p1	0.048880	40	s3	0.047060

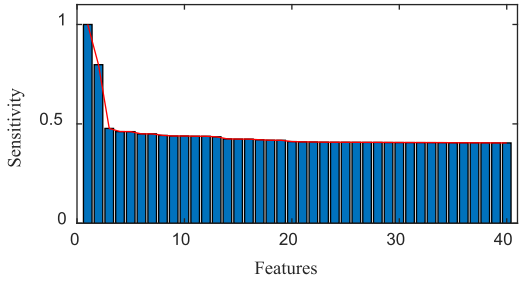

FIGURE 19. Feature sensitivity ranking.

Among the extracted new indicators, the effect of backlash on the variable-speed current signal can be observed, but it can also be seen in the figure that at some points, the indicators have crossovers, not very clear. According to the polynomial fitting theory, the reciprocal of the time interval between the shifting peak points under each type of backlash condition is taken as the ordinate y_i and the number of peaks is taken as x_i,a set of known data $\{(x_i, y_i)\ , i = 0, 1, 2, \cdots, N\}$ is established. Corresponding polynomial functions were fitted in the rising phase and the falling phase, respectively. Polynomial fitting can eliminate some singular points in the new index curve. The fitted curve is used as a more obvious index to describe different backlash.

TABLE 6. 6.25N.m feature sensitivity ranking.

Ranking	Feature	Sensitivity	Ranking	Feature	Sensitivity
1	wpd7	1	21	emd2	0.409516
2	wpd8	0.797737	22	p7	0.409026
3	s5	0.477288	23	s10	0.408043
4	s8	0.461332	24	p8	0.407724
5	s14	0.461133	25	p9	0.407670
6	s11	0.449820	6	p3	0.407329
7	s13	0.449820	27	wpd2	0.407050
8	s2	0.442119	28	wpd1	0.407004
9	p1	0.439083	29	wpd3	0.406560
10	p2	0.439056	30	p4	0.406368
11	s4	0.437932	31	p5	0.406225
12	s6	0.437727	32	p13	0.406095
13	s12	0.435030	33	wpd5	0.405953
14	s9	0.424527	34	wpd4	0.405837
15	wpd6	0.423553	35	p15	0.405121
16	s1	0.423458	36	emd2	0.404999
17	p10	0.420138	37	p12	0.404945
18	s7	0.417917	38	p11	0.40479
19	p14	0.417585	39	p6	0.404357
20	emd1	0.411059	40	s3	0.4043

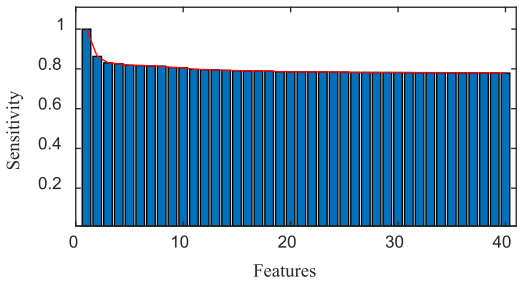

FIGURE 20. Feature sensitivity ranking.

TABLE 7. 0N.m feature sensitivity ranking.

Ranking	Feature	Sensitivity	Ranking	Feature	Sensitivity
1	wpd8	1	21	p1	0.409516
2	wpd7	0.862913	22	p3	0.409026
3	p5	0.830774	23	wpd1	0.408043
4	wpd6	0.825799	24	s10	0.784996
5	wpd3	0.818286	25	emd1	0.784825
6	s5	0.816952	26	p7	0.784567
7	p12	0.814683	27	p9	0.784190
8	p4	0.813497	28	emd2	0.783967
9	p11	0.806904	29	s14	0.782266
10	p14	0.806138	30	s1	0.782215
11	p6	0.797683	31	wpd5	0.782018
12	s8	0.796250	32	p10	0.781901
13	s12	0.795504	33	s11	0.781751
14	P8	0.792532	34	s13	0.781549
15	wpd4	0.791224	35	p13	0.781186
16	s9	0.789819	36	s6	0.781153
17	emd3	0.789262	37	s4	0.781153
18	wpd2	0.788847	38	s2	0.780646
19	p15	0.785778	39	s7	0.780011
20	p2	0.785020	40	s3	0.780010

According to the principle of polynomial fitting, χ^2 is the smallest after fitting. During the deceleration and declining stage, χ^2 is the smallest under 4-term polynomial fitting. In the accelerated rising phase, the corresponding χ^2 is the smallest under 6-term polyphase fitting. Table 8 is the 4-term polynomial coefficients fitted by the motor during

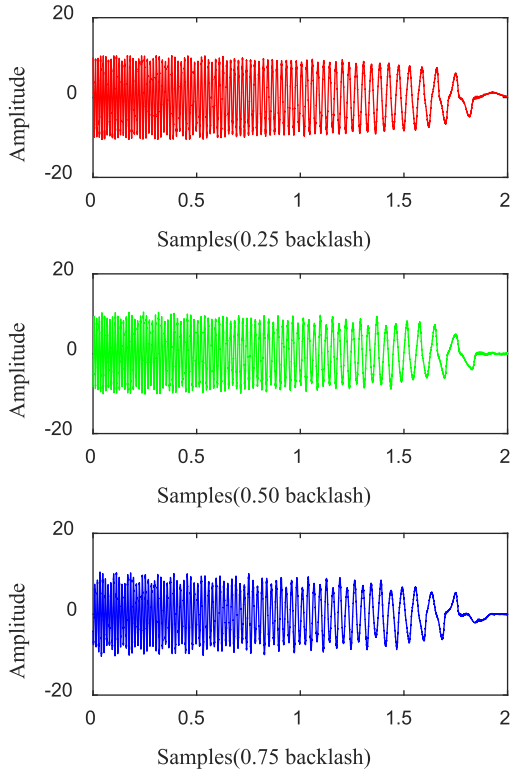

FIGURE 21. Deceleration current signal.

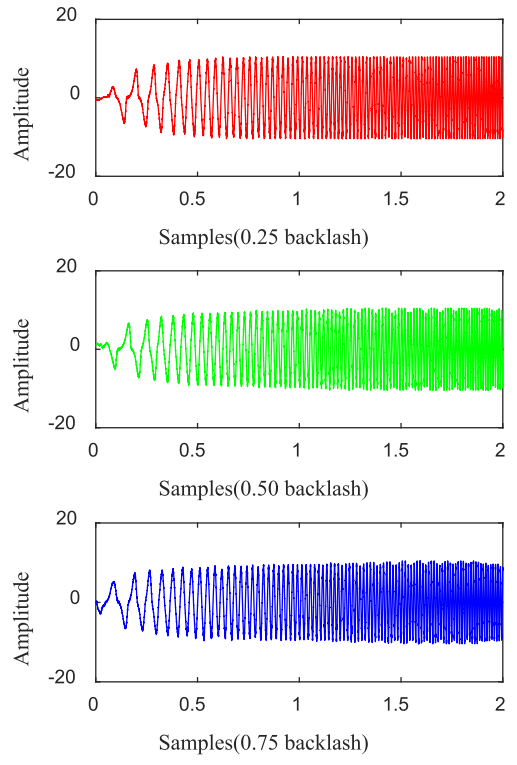

FIGURE 22. Acceleration current signal.

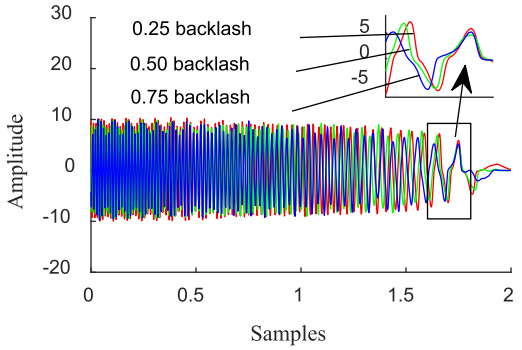

FIGURE 23. Time domain overlap.

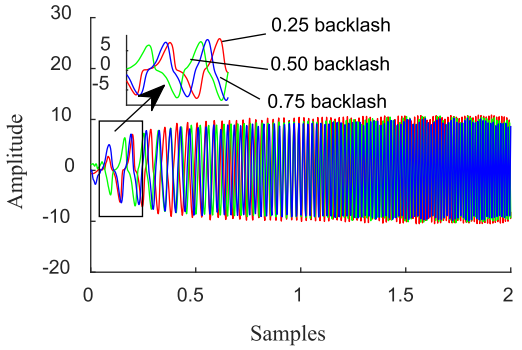

FIGURE 24. Time domain overlap.

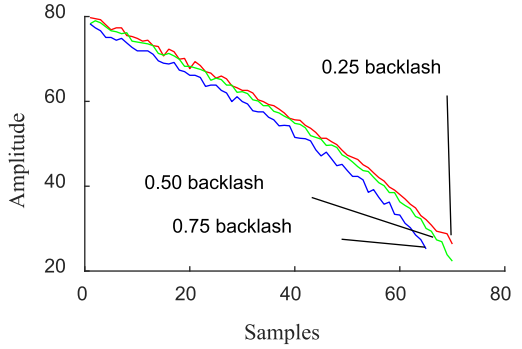

FIGURE 25. Peak interval reciprocal.

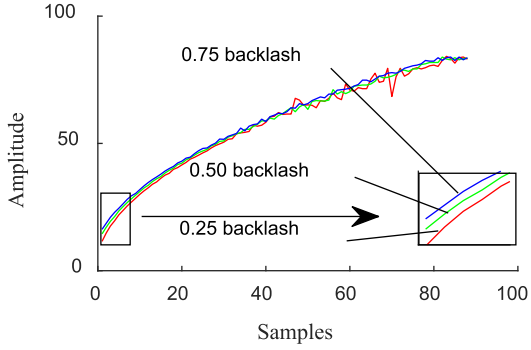

FIGURE 26. Peak interval reciprocal.

deceleration and descent under different backlash conditions. Table 9 is the 6-phase polyphase coefficients fitted under different backlash conditions during acceleration and ascent. Fig. 27 and Fig. 28 are the fitted curves. It can be seen that

TABLE 8. Polynomial fitting coefficient.

Backlash	$a4$	$a3$	$a2$	$a1$	$a0$
0.25mm	-3.51E-06	0.000497	-0.0257	-0.12478	79.92952
0.50mm	-2.72E-06	0.000303	-0.01423	-0.33436	80.06727
0.75mm	-3.40E-06	0.000377	-0.0173	-0.29802	78.12143

TABLE 9. Polynomial fitting coefficient.

Backlash	$a6$	$a5$	$a4$	$a3$	$a2$	$a1$	$a0$
0.25mm	-2.67E-09	7.52E-07	-8.27E-05	0.004525	-0.13606	3.083498	9.079022
0.50mm	-1.91E-09	5.15E-07	-5.50E-05	0.003025	-0.09705	2.606016	12.25401
0.75mm	-1.67E-09	4.49E-07	-4.82E-05	0.00268	-0.08711	2.436013	14.18497

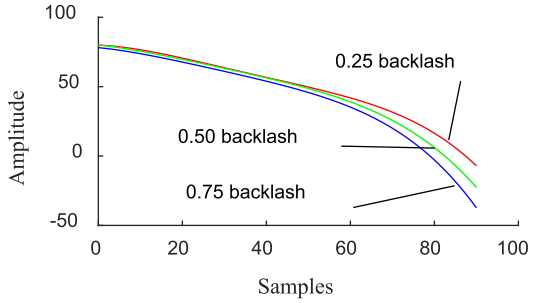

FIGURE 27. Four-term polynomial fitting.

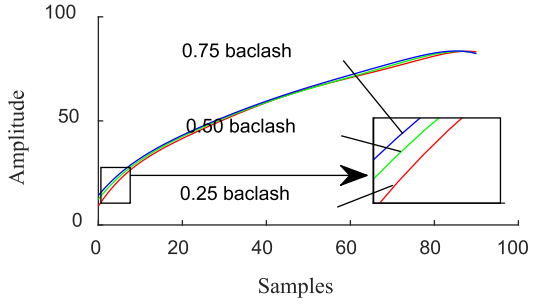

FIGURE 28. Six-term polynomial fitting.

comparing with Fig. 25 and Fig. 26, Fig. 27 and Fig. 28 has removed some dead pixels, and the curves are smoother and can clearly reflect the state of the system. Can be used as an effective feature to distinguish between different backlash.

V. CONCLUSION

Aiming at the problem of backlash of gears, this paper designs and builds a test bench. Simulate the working conditions of the gears in different backlash, and synchronously collect the three-phase current of the servo motor through the current sensor. The influence of the backlash on the stator current signal of the servo permanent magnet synchronous motor is analyzed from the collected current signal. During the stable operation of the system, the collected signals are segmented, and then multiple features are extracted in the time and frequency domains. Using the FDA to perform sensitivity ranking on the extracted features, find the features most sensitive to the backlash of the gear, which can effectively distinguish the effect of different backlash on the motor current.

In the system variable speed phase, the first is to overlap the collected current signals in the time domain, and the second is to take the reciprocal of the time interval between the peaks of the time domain signals and make a graph and fit a polynomial to its variation curve. From the fitted curves, different states of the system can be clearly distinguished. The fitted polynomial coefficient is used as an index of the effect of different backlash on the speed of the motor. The analysis of experimental data shows that this index is highly sensitive to the backlash of gears, and it can distinguish the conditions of different backlash. It can be used as an effective index to characterize the effect of different backlash on the variable speed operation of the motor.

The existence of gear meshing backlash has a great impact on the system. This article explores the impact of different gear backlash on the drive system and stator current through experiments. The current state of the gear is used as a research object to monitor the health of the gear drive system. Provide practical references.

REFERENCES

[1] A. R. Mohanty and C. Kar, "Fault detection in a multistage gearbox by demodulation of motor current waveform," *IEEE Trans. Ind. Electron.*, vol. 53, no. 4, pp. 1285–1297, Jun. 2006.

[2] K. Feng, P. Borghesani, W. A. Smith, R. B. Randall, Z. Y. Chin, J. Ren, and Z. Peng, "Vibration-based updating of wear prediction for spur gears," *Wear*, vols. 426–427, pp. 1410–1415, Apr. 2019.

[3] T. Ouyang, H. Huang, X. Zhou, M. Pan, N. Chen, and D. Lv, "A finite line contact tribo-dynamic model of a spur gear pair," *Tribology Int.*, vol. 119, pp. 753–765, Mar. 2018.

[4] X. Xu, Z. Yu, and H. Ding, "Failure analysis of a diesel engine gear-shaft," *Eng. Failure Anal.*, vol. 13, no. 8, pp. 1351–1357, Dec. 2006.

[5] Z. Yu and X. Xu, "Failure investigation of a truck diesel engine gear train consisting of crankshaft and camshaft gears," *Eng. Failure Anal.*, vol. 17, no. 2, pp. 537–545, Mar. 2010.

[6] X. Yu, L. Feng, H. Wang, and Y. He, "Fracture failure analysis of 12Cr2Ni4 steel gear," *Heat Treat. Metals*, vol. 40, no. 11, pp. 191–194, Nov. 2015.

[7] E. Caso, A. Fernandez-del-Rincon, P. Garcia, M. Iglesias, and F. Viadero, "Monitoring of misalignment in low speed geared shafts with acoustic emission sensors," *Appl. Acoust.*, vol. 159, Feb. 2020, Art. no. 107092.

[8] M. A. Khan, M. A. Shahid, S. A. Ahmed, S. Z. Khan, K. A. Khan, S. A. Ali, and M. Tariq, "Gear misalignment diagnosis using statistical features of vibration and airborne sound spectrums," *Measurement*, vol. 145, pp. 419–435, Oct. 2019.

[9] M. Amarnath and I. R. P. Krishna, "Detection and diagnosis of surface wear failure in a spur geared system using EEMD based vibration signalanalysis," *Tribology Int.*, vol. 61, pp. 224–234, May 2013.

[10] Y. Yi, K. Huang, Y. Xiong, and M. Sang, "Nonlinear dynamic modelling and analysis for a spur gear system with time-varying pressure angle and gear backlash," *Mech. Syst. Signal Process.*, vol. 132, pp. 18–34, Oct. 2019.

[11] J.-F. Shi, X.-F. Gou, and L.-Y. Zhu, "Modeling and analysis of a spur gear pair considering multi-state mesh with time-varying parameters and backlash," *Mechanism Mach. Theory*, vol. 134, pp. 582–603, Apr. 2019.

[12] Q. Chen, Y. Ma, S. Huang, and H. Zhai, "Research on gears' dynamic performance influenced by gear backlash based on fractal theory," *Appl. Surf. Sci.*, vol. 313, pp. 325–332, Sep. 2014.

[13] Y. Shen, S. Yang, and X. Liu, "Nonlinear dynamics of a spur gear pair with time-varying stiffness and backlash based on incremental harmonic balance method," *Int. J. Mech. Sci.*, vol. 48, no. 11, pp. 1256–1263, Nov. 2006.

[14] M. Kuai, G. Cheng, Y. Pang, and Y. Li, "Research of planetary gear fault diagnosis based on permutation entropy of CEEMDAN and ANFIS," *Sensors*, vol. 18, no. 3, p. 782, Mar. 2018.

[15] H. Mahgoun, R. E. Bekka, and A. Felkaoui, "Gearbox fault diagnosis using ensemble empirical mode decomposition (EEMD) and residual signal," *Mech. Ind.*, vol. 13, no. 1, pp. 33–44, 2012.

[16] S. Park, S. Kim, and J.-H. Choi, "Gear fault diagnosis using transmission error and ensemble empirical mode decomposition," *Mech. Syst. Signal Process.*, vol. 108, pp. 262–275, Aug. 2018.

[17] V. Atamuradov, K. Medjaher, P. Dersin, B. Lamoureux, and N. Zerhouni, "Prognostics and health management for maintenance practitioners-review, implementation and tools evaluation," *Int. J. Prognostics Health Manage.*, vol. 8, pp. 1–31, Dec. 2017.

[18] Y. Zhang, C. Zhang, J. Sun, and J. Guo, "Improved wind speed prediction using empirical mode decomposition," *Adv. Elect. Comput. Eng.*, vol. 18, no. 2, pp. 3–10, 2018.

[19] Y. Miao, M. Zhao, K. Liang, and J. Lin, "Application of an improved MCKDA for fault detection of wind turbine gear based on encoder signal," *Renew. Energy*, vol. 151, pp. 192–203, May 2020.

[20] M. Zhao, X. Jia, J. Lin, Y. Lei, and J. Lee, "Instantaneous speed jitter detection via encoder signal and its application for the diagnosis of planetary gearbox," *Mech. Syst. Signal Process.*, vol. 98, pp. 16–31, Jan. 2018.

[21] J. Yu and Y. He, "Planetary gearbox fault diagnosis based on data-driven valued characteristic multigranulation model with incomplete diagnostic information," *J. Sound Vib.*, vol. 429, pp. 63–77, Sep. 2018.

[22] A. Ibrahim, M. El Badaoui, F. Guillet, and F. Bonnardot, "A new bearing fault detection method in induction machines based on instantaneous power factor," *IEEE Trans. Ind. Electron.*, vol. 55, no. 12, pp. 4252–4259, Dec. 2008.

[23] Q. Zhang, L. Tan, and G. Xu, "Evaluating transient performance of servo mechanisms by analysing stator current of PMSM," *Mech. Syst. Signal Process.*, vol. 101, pp. 535–548, Feb. 2018.

[24] X. Li, G. Ouyang, and Z. Liang, "Complexity measure of motor current signals for tool flute breakage detection in end milling," *Int. J. Mach. Tools Manuf.*, vol. 48, nos. 3–4, pp. 371–379, Mar. 2008.

[25] M. Soualhi, K. T. P. Nguyen, A. Soualhi, K. Medjaher, and K. E. Hemsas, "Health monitoring of bearing and gear faults by using a new health indicator extracted from current signals," *Measurement*, vol. 141, pp. 37–51, Jul. 2019.

[26] F. Li, X. Pang, and Z. Yang, "Motor current signal analysis using deep neural networks for planetary gear fault diagnosis," *Measurement*, vol. 145, pp. 45–54, Oct. 2019.

[27] R. Zhang, F. Gu, H. Mansaf, T. Wang, and A. D. Ball, "Gear wear monitoring by modulation signal bispectrum based on motor current signal analysis," *Mech. Syst. Signal Process.*, vol. 94, pp. 202–213, Sep. 2017.

[28] R. R. Obaid, T. G. Habetler, and R. M. Tallam, "Detecting load unbalance and shaft misalignment using stator current in inverter-driven induction motors," in *Proc. IEEE Int. Electr. Mach. Drives Conf. (IEMDC)*, Jun. 2003, pp. 1454–1458.

[29] J. Zhang, J. S. Dhupia, and C. J. Gajanayake, "Stator current analysis from electrical machines using resonance residual technique to detect faults in planetary gearboxes," *IEEE Trans. Ind. Electron.*, vol. 62, no. 9, pp. 5709–5721, Sep. 2015.

[30] A. Picot, Z. Obeid, J. Régnier, S. Poignant, O. Darnis, and P. Maussion, "Statistic-based spectral indicator for bearing fault detection in permanent-magnet synchronous machines using the stator current," *Mech. Syst. Signal Process.*, vol. 46, no. 2, pp. 424–441, Jun. 2014.

[31] C. Verucchi, J. Bossio, G. Bossio, and G. Acosta, "Misalignment detection in induction motors with flexible coupling by means of estimated torque analysis and MCSA," *Mech. Syst. Signal Process.*, vol. 80, pp. 570–581, Dec. 2016.

[32] Z. Li, G. Tan, and Y. Li, "Fault diagnosis based on improved kernel Fisher discriminant analysis," *J. Softw.*, vol. 7, no. 12, pp. 2657–2662, Dec. 2012.

[33] N. M. Nor, M. A. Hussain, and C. R. C. Hassan, "Process monitoring and fault detection in non-linear chemical process based on multi-scale kernel Fisher discriminant analysis," in *Proc. 12th Int. Symp. Process Syst. Eng. 25th Eur. Symp. Comput. Aided Process Eng. B, Comput.-Aided Process Eng.*, Lyngby, Denmark, 2015, pp. 1823–1828.

[34] H.-W. Cho, "Identification of contributing variables using kernel-based discriminant modeling and reconstruction," *Expert Syst. Appl.*, vol. 33, no. 2, pp. 274–285, Aug. 2007.

[35] Z.-B. Zhu and Z.-H. Song, "Fault diagnosis based on imbalance modified kernel Fisher discriminant analysis," *Chem. Eng. Res. Design*, vol. 88, no. 8, pp. 936–951, Aug. 2010.

[36] Z.-B. Zhu and Z.-H. Song, "A novel fault diagnosis system using pattern classification on kernel FDA subspace," *Expert Syst. Appl.*, vol. 38, no. 6, pp. 6895–6905, Jun. 2011.

[37] S. Morimoto, Y. Takeda, and T. Hirasa, "Current phase control methods for permanent magnet synchronous motors," *IEEE Trans. Power Electron.*, vol. 5, no. 2, pp. 133–139, Apr. 1990.

QICHAO YANG received the B.S. degree in mechanical engineering from the Kunming University of Science and Technology, China, in 2018, where he is currently pursuing the master's degree with the Faculty of Mechanical and Electrical Engineering. His research interest includes fault diagnosis of gears and bearings from electrical signals.

TAO LIU received the Ph.D. degree in engineering from the State Key Laboratory of Mechanical System and Vibration, Shanghai Jiao Tong University, in April 2014. He lectures on machinery fault diagnosis for master's and Ph.D. students. In the past five years, he has hosted or participated in more than ten scientific research projects and has published more than 20 articles, including as the first/corresponding author, he has published more than ten SCI/EI indexed articles. His current research interests include modern signal processing theory and methods, intelligent diagnosis of industrial equipment, equipment performance evaluation, and life prediction application. He is also a member of the Fault Diagnosis Professional Committee of the Chinese Society of Vibration Engineering.

XING WU received the Ph.D. degree in engineering from the State Key Laboratory of Mechanical System and Vibration, Shanghai Jiao Tong University, majoring in mechanical design and theory, in 2005. He was an International Third-Level Vibration Analyst, reserve talents for young and middle-aged academic and technical leaders in Yunnan Province; a 2018–2022 member of the Higher Education Machinery Committee of the Ministry of Education; the Director of the 2018–2022 Higher Education Machinery Committee of Yunnan Province; the Intelligent Maintenance of Advanced Equipment in Yunnan Province Director of the Engineering Research Center, and the Director of the Yunnan Provincial Key Laboratory of Vibration and Noise. He concurrently serves as the Director of the Chinese Society of Vibration Engineering, the Executive Director of the Fault Diagnosis Professional Committee of the Chinese Society of Vibration Engineering, and the Vice Chairman of the Yunnan Mechanical Engineering Society.

YUNNAN DENG received the B.S. degree in mechanical engineering from Shanghai University, China, in 2018. He is currently pursuing the master's degree with the Faculty of Mechanical and Electrical Engineering, Kunming University of Science and Technology His research interest includes system parameters identification based on torsional vibration signal.